Commun. Comput. Phys.
doi: 10.4208/cicp.140811.060112a

Vol. **12**, No. 5, pp. 1461-1481
November 2012

Numerical Simulation of a Weakly Nonlinear Model for Internal Waves

Robyn Canning Gregory and David P. Nicholls*

Department of Mathematics, Statistics and Computer Science, University of Illinois at Chicago, Chicago, IL 60607, USA.

Received 14 August 2011; Accepted (in revised version) 6 January 2012

Communicated by Jie Shen

Available online 8 May 2012

Abstract. Internal waves arise in a wide array of oceanographic problems of both theoretical and engineering interest. In this contribution we present a new model, valid in the weakly nonlinear regime, for the propagation of disturbances along the interface between two ideal fluid layers of infinite extent and different densities. Additionally, we present a novel high-order/spectral algorithm for its accurate and stable simulation. Numerical validation results and simulations of wave-packet evolution are provided.

AMS subject classifications: 76B07, 76B15, 76B55, 65M70

Key words: Internal waves, weakly nonlinear waves, high-order spectral methods, Dirichlet Neumann operators, surface formulation.

1 Introduction

An internal water-wave propagates along an interface between two fluids with varying densities due to variations in temperature and salinity [18]. Internal waves are ubiquitous in the world's oceans and, as seen by satellite [15], they have been observed to travel for hundreds of miles within the oceans. Internal waves are important both as a significant source of energy and momentum transportation and in their interactions with ocean dynamics and topographies. In addition to their many engineering and other practical applications, they inspire many difficult questions in both theoretical and numerical analysis.

*Corresponding author. *Email addresses:* rcanni2@uic.edu (R. C. Gregory), nicholls@math.uic.edu (D. P. Nicholls)

The classical formulation of the internal water-wave problem uses Euler's equations with kinematic and dynamic boundary conditions at the free interface. Well-known approximation models include, most notably, the Korteweg-de Vries, Benjamin-Ono, Boussinesq, Nonlinear Schrödinger and Intermediate Long Wave equations [4, 25]. Alternatively, one could reformulate the classical system as a boundary integral equation, a Hamiltonian system, or as evolution equations involving operators (see, e.g., [7, 13] for recent examples).

This paper is a numerical study of time-dependent internal wave propagation and for this we focus on two-fluid systems which Koop & Butler [16] believe are sufficient to capture the physics of the problem. For simplicity, we neglect forces other than gravity and assume infinite extent in both the upper and lower layers, but we note that our method can easily be extended to include additional forces (e.g., surface tension), finite layers and rigid-lid assumptions. The model derivation is based on a perturbative approach [26] in the weakly nonlinear regime (see also [5, 25]) and our evolution equations govern interface variables involving interface integral operators, e.g., Dirichlet-Neumann operators (DNOs). The interface variables, first introduced by Benjamin & Bridges [1, 2] and Craig & Groves [6], are analogous to the surface variables identified by Zakharov [33] for a Hamiltonian formulation of the classical single-fluid water-wave problem. The DNO, a linear operator that maps Dirichlet boundary data to Neumann boundary data [27] was introduced to the water-wave problem by Craig and Sulem [10] (see also the work of Milder [20, 21] and Milder & Sharp [22, 23] in the setting of electromagnetic scattering) to make Zakharov's formulation more explicit. The interface formulation is appealing for a number of reasons, not the least of which is that it reduces the problem dimension. In [10] Craig and Sulem used the new formulation to numerically simulate surface gravity waves. Our work is motivated by [6, 10] and can be considered both an extension of their work to the two-fluid case and a complement to the research of [7, 11] who also use this formulation for such simulations.

To the authors' knowledge, this work presents, for the first time, numerical simulations of truncated Dirichlet-Neumann operators which have not appeared in the literature before. We also point out that due to the interface formulation and the spectrally accurate nature of our algorithm, our approach *cannot* be surpassed in terms of accuracy and speed (though integral equation approaches will have roughly the same operation counts).

Given our model equations, the evolution of the internal wave is simulated by a Fourier collocation spectral method [12] in the spatial variable and a fourth-order Runge-Kutta algorithm [3] for time-stepping. The main effort lies with the approximation of the operators and once this is accomplished, the numerical method is fast, highly accurate and easy to implement. The full literature of numerical schemes to simulate the motion of a free surface or interface in the Euler equations of ideal fluid motion is far too vast to recapitulate here. For the interested reader we recommend the survey articles of [14, 19, 30–32].

This paper is organized as follows: In Section 2.1 we outline the classical formulation

of the problem and in Section 2.2 we reformulate the problem in terms of interface variables and interface integral operators. In Section 2.3 we describe a Boundary Perturbation Method (the method of Operator Expansions-OE) to simulate the interface operators and, after nondimensionalizing, we present our model equations in Section 2.4. In Section 3.1 we describe our numerical method and in Section 3.2 we derive exact solutions that are used to test our code. We present numerical results in Section 4.

2 Derivation of the model equations

2.1 Equations of motion

Consider two-dimensional ideal fluid flow in the deep ocean where an interface well below the ocean surface separates two layers of varying densities. Assume the fluids are immiscible with densities ρ' and ρ ($\rho>\rho'$) in the top and bottom layers, respectively. Denoting the layer interface by $y=\eta(x,t)$, we define the fluid domains in the upper and lower regions by

$$S':=\{(x,y)\in\mathbf{R}\times\mathbf{R}\mid y>\eta(x,t)\},\qquad S:=\{(x,y)\in\mathbf{R}\times\mathbf{R}\mid y<\eta(x,t)\},$$

see Fig. 1.

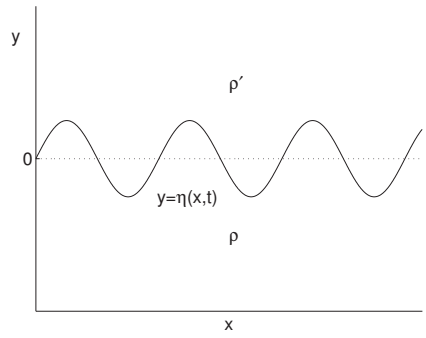

Figure 1: Domain of the internal water-wave problem.

Recall that an ideal fluid is incompressible, irrotational and inviscid [18] and that irrotationality implies that there exists a velocity potential in each region such that

$$\begin{aligned}\mathbf{u}'(x,y,t)&=\nabla\phi'(x,y,t),\qquad \text{in } S',\\ \mathbf{u}(x,y,t)&=\nabla\phi(x,y,t),\qquad \text{in } S,\end{aligned}$$

where $\mathbf{u}'$ and $\mathbf{u}$ are the velocities in the upper and lower layers, respectively. As a result of the incompressibility condition, the potential functions satisfy Laplace's equation in their domains of definition:

$$\begin{aligned}\Delta\phi'&=0,\qquad \text{in } S',\\ \Delta\phi&=0,\qquad \text{in } S.\end{aligned}$$

To specify a unique solution we require lateral and vertical boundary conditions for our fluid flow. For the former we consider the classical λ-periodicity conditions

$$\eta(x+\lambda,t)=\eta(x,t),\quad \phi'(x+\lambda,y,t)=\phi'(x,y,t),\quad \phi(x+\lambda,y,t)=\phi(x,y,t),\quad \forall x\in\mathbf{R}.$$

As we have assumed fluids of infinite extent, we specify that the velocity vanishes far from the interface:

$$\begin{aligned}&\partial_y\phi'\to 0, &&\text{as } y\to\infty,\\ &\partial_y\phi\to 0, &&\text{as } y\to-\infty.\end{aligned}$$

The kinematic condition at the interface gives

$$\begin{aligned}\partial_t\eta&=\partial_y\phi'-(\partial_x\eta)\partial_x\phi',\\ \partial_t\eta&=\partial_y\phi-(\partial_x\eta)\partial_x\phi.\end{aligned}$$

The pressure balance, or Bernoulli's condition, at the interface produces

$$\rho'\Big(\partial_t\phi'+\frac{1}{2}|\nabla\phi'|^2+g\eta\Big)=\rho\Big(\partial_t\phi+\frac{1}{2}|\nabla\phi|^2+g\eta\Big),$$

where g is the acceleration due to gravity. Collecting all of the constraints above, the full system of equations are given by

$$\begin{aligned}&\Delta\phi'=0, && \text{in } S', && (2.1a)\\ &\partial_y\phi'\to 0, && y\to\infty, && (2.1b)\\ &\partial_t\eta=\partial_y\phi'-(\partial_x\eta)\partial_x\phi', && \text{at } y=\eta, && (2.1c)\\ &\Delta\phi=0, && \text{in } S, && (2.1d)\\ &\partial_y\phi\to 0, && y\to-\infty, && (2.1e)\\ &\partial_t\eta=\partial_y\phi-(\partial_x\eta)\partial_x\phi, && \text{at } y=\eta, && (2.1f)\\ &\rho'\Big(\partial_t\phi'+\frac{1}{2}|\nabla\phi'|^2+g\eta\Big)=\rho\Big(\partial_t\phi+\frac{1}{2}|\nabla\phi|^2+g\eta\Big), && \text{at } y=\eta, && (2.1g)\end{aligned}$$

which should be supplemented with initial conditions for η, ϕ and ϕ'.

2.2 Interface variables and Dirichlet-Neumann operators

Now we reformulate system (2.1) in terms of interfacial variables and interface operators (Dirichlet-Neumann operators). Following Benjamin & Bridges [1, 2] and Craig & Groves [6], we define

$$\xi(x,t):=\rho\Phi(x,t)-\rho'\Phi'(x,t),$$

where

$$\Phi(x,t):=\phi(x,\eta(x,t),t),\qquad \Phi'(x,t):=\phi'(x,\eta(x,t),t),$$

the weighted difference of the potentials on the interface. Benjamin & Bridges showed that the variables (η,ξ) form a canonical set of variables in a Hamiltonian formulation of this two-layer flow (c.f., [8, 33]) and we use these as evolution variables in our study. To find evolution equations for these, we first introduce Dirichlet-Neumann Operators (DNOs) which relate normal derivatives of the potential at the interface to these new interface quantities.

We recall [10,20,27] that a DNO maps Dirichlet data to Neumann data at the interface of a domain and two which are useful here are

$$G'(\eta)[\Phi'] := \nabla\phi'\cdot N = \nabla\phi'|_{y=\eta}\cdot(-\partial_x\eta,1) = [\partial_y\phi' - (\partial_x\eta)\partial_x\phi']_{y=\eta}, \tag{2.2a}$$
$$G(\eta)[\Phi] := \nabla\phi\cdot N = \nabla\phi|_{y=\eta}\cdot(-\partial_x\eta,1) = [\partial_y\phi - (\partial_x\eta)\partial_x\phi]_{y=\eta}, \tag{2.2b}$$

where the normal vector $N=(-\partial_x\eta,1)^T$ is exterior to the lower fluid domain and interior to the upper. With these definitions, (2.1c) and (2.1f) become

$$\partial_t\eta = G'(\eta)[\Phi'], \tag{2.3a}$$
$$\partial_t\eta = G(\eta)[\Phi], \tag{2.3b}$$

which also imply that the DNOs are equal (i.e., there can be no jump in the normal component of velocity at the interface). Using the definition of ξ, the linear properties of the DNO and the equality of the DNOs, we have

$$G(\eta)[\xi] = (\rho G'(\eta) - \rho' G(\eta))[\Phi'], \tag{2.4a}$$
$$G'(\eta)[\xi] = (\rho G'(\eta) - \rho' G(\eta))[\Phi]. \tag{2.4b}$$

If we define a new operator $B(\eta)=\rho G'(\eta)-\rho' G(\eta)$, then from (2.4)

$$\Phi' = B^{-1}(\eta)G(\eta)[\xi], \tag{2.5a}$$
$$\Phi = B^{-1}(\eta)G'(\eta)[\xi]. \tag{2.5b}$$

Plugging (2.5) into (2.3) we arrive at two possible evolution equations for η:

$$\partial_t\eta = G'(\eta)B^{-1}(\eta)G(\eta)[\xi], \tag{2.6a}$$
$$\partial_t\eta = G(\eta)B^{-1}(\eta)G'(\eta)[\xi]. \tag{2.6b}$$

Seeking an equation for the time evolution of ξ we compute

$$\partial_t\xi = \partial_t[\rho\Phi - \rho'\Phi'].$$

An application of the chain rule (and a substitution from (2.1g)) gives

$$\partial_t\xi = -(\rho-\rho')g\eta - \frac{1}{2}\rho|\nabla\phi|^2 + \frac{1}{2}\rho'\left|\nabla\phi'\right|^2 + \rho\partial_y\phi\partial_t\eta - \rho'\partial_y\phi'\partial_t\eta. \tag{2.7}$$

If we replace $\partial_t\eta$ by either of the terms in (2.6), then we simply need expressions for $\partial_x\phi$ and $\partial_y\phi$ in terms of η and ξ to close our system of equations. Another application of the chain rule delivers

$$\partial_x\Phi=\partial_x\phi+(\partial_x\eta)\partial_y\phi,$$

and Eq. (2.2b) gives the system

$$\begin{pmatrix}1 & \partial_x\eta\\ -\partial_x\eta & 1\end{pmatrix}\begin{pmatrix}\partial_x\phi\\ \partial_y\phi\end{pmatrix}=\begin{pmatrix}\partial_x\Phi\\ G(\eta)[\Phi]\end{pmatrix}.$$

Consequently,

$$\begin{pmatrix}\partial_x\phi\\ \partial_y\phi\end{pmatrix}=\frac{1}{1+(\partial_x\eta)^2}\begin{pmatrix}\partial_x\Phi-(\partial_x\eta)G(\eta)[\Phi]\\ (\partial_x\eta)\partial_x\Phi+G(\eta)[\Phi]\end{pmatrix} \tag{2.8}$$

and analogously,

$$\begin{pmatrix}\partial_x\phi'\\ \partial_y\phi'\end{pmatrix}=\frac{1}{1+(\partial_x\eta)^2}\begin{pmatrix}\partial_x\Phi'-(\partial_x\eta)G'(\eta)[\Phi']\\ (\partial_x\eta)\partial_x\Phi'+G'(\eta)[\Phi']\end{pmatrix}. \tag{2.9}$$

Substituting (2.5), (2.8) and (2.9) into (2.7) yields an evolution equation for ξ:

$$\begin{aligned}\partial_t\xi=&-(\rho-\rho')g\eta+\frac{1}{2(1+(\partial_x\eta)^2)}\Big\{-\rho\big(\partial_xB^{-1}(\eta)G'(\eta)[\xi]\big)^2\\ &+\rho\big(G(\eta)B^{-1}(\eta)G'(\eta)[\xi]\big)^2+2\rho\partial_x\eta\big(\partial_xB^{-1}(\eta)G'(\eta)[\xi]\big)\big(G(\eta)B^{-1}(\eta)G'(\eta)[\xi]\big)\\ &+\rho'\big(\partial_xB^{-1}(\eta)G(\eta)[\xi]\big)^2-\rho'\big(G'(\eta)B^{-1}(\eta)G(\eta)[\xi]\big)^2\\ &-2\rho'\partial_x\eta\big(\partial_xB^{-1}(\eta)G(\eta)[\xi]\big)\big(G'(\eta)B^{-1}(\eta)G(\eta)[\xi]\big)\Big\}.\end{aligned} \tag{2.10}$$

2.3 Operator expansions

The only specification remaining is the computation of the operators $G(\eta)$, $G'(\eta)$ and $B^{-1}(\eta)$. For this we choose a convenient and accurate Boundary Perturbation Method: the method of Operator Expansions (OE) [10, 20–23]. This approach is based on the smooth dependence of the DNO upon sufficiently small boundary deformations, e.g.,

$$\eta(x,t)=\epsilon\tilde{\eta}(x,t),\qquad \epsilon\ll 1.$$

More specifically, Coifman & Meyer [9] (see also Nicholls & Reitich [27]) proved that the operators G and G' are analytic functions of Lipschitz deformations η, so that they can be expanded as convergent Taylor series:

$$G(\eta)[\xi]=G(\epsilon\tilde{\eta})[\xi]=\sum_{n=0}^{\infty}G_n(\tilde{\eta})[\xi]\epsilon^n,\qquad G'(\eta)[\xi]=G'(\epsilon\tilde{\eta})[\xi]=\sum_{n=0}^{\infty}G'_n(\tilde{\eta})[\xi]\epsilon^n. \tag{2.11}$$

These results can be extended to the operators B and $M:=B^{-1}$ so that

$$M(\eta)[\xi]=M(\epsilon\tilde{\eta})[\xi]=\sum_{n=0}^{\infty}M_n(\tilde{\eta})[\xi]\epsilon^n.$$

The OE method delivers high order formulas for the Taylor series terms (e.g., G_n) which can then be used in a *spectrally* accurate approximation, for instance

$$G(\eta)\approx G^N(\eta):=\sum_{n=0}^{N}G_n(\tilde{\eta})[\xi]\epsilon^n.$$

The derivation of formulas for the G_n have been given in a number of publications [10, 20, 27], but we include them up to order one for completeness. To begin, we note that

$$\phi_p'(x,y)=e^{ipx-|p|y},\qquad \phi_p(x,y)=e^{ipx+|p|y}$$

are $\lambda=2\pi$-periodic solutions of (2.1a)-(2.1b) and (2.1d)-(2.1e), respectively, for any integer p. Inserting ϕ_p into the definition of the DNO G, (2.2b), we find

$$G(\epsilon\tilde{\eta})\left[e^{ipx+|p|\epsilon\tilde{\eta}}\right]=[|p|-\partial_x(\epsilon\tilde{\eta})(ip)]e^{ipx+|p|\epsilon\tilde{\eta}}.$$

Using the Taylor series for G, (2.11) and expanding the exponentials in a Taylor series in ϵ, we obtain, after dropping the tildes,

$$\Big(\sum_{n=0}^{\infty}G_n(\eta)[\xi]\epsilon^n\Big)\Big[e^{ipx}\sum_{n=0}^{\infty}\frac{\eta^n}{n!}|p|^n\epsilon^n\Big]=[|p|-\epsilon\partial_x\eta(ip)]e^{ipx}\Big[\sum_{n=0}^{\infty}\frac{\eta^n}{n!}|p|^n\epsilon^n\Big].$$

Equating at order zero,

$$G_0(\eta)[e^{ipx}]=|p|e^{ipx},$$

and at order one,

$$G_1(\eta)[e^{ipx}]=\Big[\eta|p|^2-(\partial_x\eta)ip\Big]e^{ipx}-G_0(\eta)[\eta|p|e^{ipx}],$$

which, as we shall see, suffice for the purposes of this paper; higher order terms can be easily recovered if desired and useful formulas can be found in, e.g., [27].

Similar manipulations for ϕ' and G' reveal

$$\begin{aligned}G_0'(\eta)[e^{ipx}]&=-|p|e^{ipx},\\ G_1'(\eta)[e^{ipx}]&=\left[\eta|p|^2-(\partial_x\eta)ip\right]e^{ipx}-G_0'(\eta)[-\eta|p|e^{ipx}].\end{aligned}$$

If we define the Fourier multiplier $D:=(1/i)\partial_x$ and write ξ as a Fourier series,

$$\xi(x)=\sum_{p=-\infty}^{\infty}\hat{\xi}_p e^{ipx},\qquad \hat{\xi}_p=\frac{1}{2\pi}\int_0^{2\pi}\xi(x)e^{-ipx}dx,$$

then,

$$G_0[\xi] = |D|\xi, \tag{2.12a}$$
$$G_0'[\xi] = -|D|\xi, \tag{2.12b}$$
$$G_1(\eta)[\xi] = \eta|D|^2\xi - (\partial_x\eta)(\partial_x\xi) - |D|[\eta|D|\xi], \tag{2.12c}$$
$$G_1'(\eta)[\xi] = \eta|D|^2\xi - (\partial_x\eta)(\partial_x\xi) - |D|[\eta|D|\xi]. \tag{2.12d}$$

To find forms for the M_n we use the fact that

$$M(\rho G' - \rho' G) = I,$$

which, upon expansion, can be written as

$$\Big(\sum_{n=0}^{\infty} M_n(\eta)[\xi]\epsilon^n\Big)\Big[\rho\sum_{n=0}^{\infty} G_n'(\eta)[\xi]\epsilon^n - \rho'\sum_{n=0}^{\infty} G_n(\eta)[\xi]\epsilon^n\Big] = I.$$

After two convolutions in perturbation order we have

$$\sum_{n=0}^{\infty}\epsilon^n\Big[\rho\sum_{l=0}^{n} M_l(\eta)G_{n-l}'(\eta)[\xi] - \rho'\sum_{l=0}^{n} M_l(\eta)G_{n-l}(\eta)[\xi]\Big] = I$$

and equating at order zero,

$$M_0(\eta)[\xi] = \big[\rho G_0'(\eta) - \rho' G_0(\eta)\big]^{-1}[\xi] = -\frac{1}{\rho+\rho'}|D|^{-1}\xi, \tag{2.13}$$

where $D^{-1} := i\int dx$. This integration operator is the right inverse of D, but is only the left inverse up to a constant. To render this a well-defined operator we restrict the range to the set of zero-mean functions. At order one,

$$\begin{aligned} M_1(\eta)[\xi] &= -M_0(\eta)\Big\{\Big(\rho G_1'(\eta) - \rho' G_1(\eta)\Big)\Big[M_0(\eta)[\xi]\Big]\Big\} \\ &= -\frac{\rho-\rho'}{(\rho+\rho')^2}|D|^{-1}\big[\eta|D|\xi - (\partial_x\eta)(\partial_x|D|^{-1}\xi) - |D|[\eta\xi]\big]. \end{aligned} \tag{2.14}$$

As our eventual goal is to find a weakly nonlinear model accurate to order two, the following operator combinations (derived from (2.12), (2.13), (2.14)) will serve our purposes:

$$G_0'M_0G_0[\xi] = \frac{1}{\rho+\rho'}|D|\xi,$$
$$G_0'M_0G_1[\xi] = \frac{1}{\rho+\rho'}\big[\eta|D|^2\xi - (\partial_x\eta)(\partial_x\xi) - |D|[\eta|D|\xi]\big],$$

$$G_0'M_1G_0[\xi]=\frac{\rho-\rho'}{(\rho+\rho')^2}\left[\eta|D|^2\xi-(\partial_x\eta)(\partial_x\xi)-|D|[\eta|D|\xi]\right],$$
$$G_1'M_0G_0[\xi]=-\frac{1}{\rho+\rho'}\left[\eta|D|^2\xi-(\partial_x\eta)(\partial_x\xi)-|D|[\eta|D|\xi]\right],$$
$$G_0M_0G_0'[\xi]=\frac{1}{\rho+\rho'}|D|\xi,$$
$$M_0G_0'[\xi]=\frac{1}{\rho+\rho'}\xi,$$
$$M_0G_0[\xi]=-\frac{1}{\rho+\rho'}\xi.$$

2.4 Nondimensionalization

At this point it is convenient to nondimensionalize our nonlinear system of equations governing (η,ξ), (2.6) and (2.10). We select (2.6a) for the evolution of η and recall that we denoted the operator B^{-1} by M, so we have

$$\partial_t\eta=G'(\eta)M(\eta)G(\eta)[\xi], \tag{2.15a}$$
$$\begin{aligned}\partial_t\xi=&-(\rho-\rho')g\eta+\frac{1}{2(1+(\partial_x\eta)^2)}\Big\{-\rho(\partial_xM(\eta)G'(\eta)[\xi])^2\\&+\rho(G(\eta)M(\eta)G'(\eta)[\xi])^2+2\rho(\partial_x\eta)(\partial_xM(\eta)G'(\eta)[\xi])(G(\eta)M(\eta)G'(\eta)[\xi])\\&+\rho'(\partial_xM(\eta)G(\eta)[\xi])^2-\rho'(G'(\eta)M(\eta)G(\eta)[\xi])^2\\&-2\rho'(\partial_x\eta)(\partial_xM(\eta)G(\eta)[\xi])(G'(\eta)M(\eta)G(\eta)[\xi])\Big\}.\end{aligned} \tag{2.15b}$$

Let $L=\lambda/2\pi$ and a be a typical length and amplitude, respectively and consider the classical scalings [18]:

$$x=L\bar{x},\qquad y=L\bar{y},\qquad \eta=a\bar{\eta}.$$

We scale time by the ratio of the linear wave speed and the length parameter,

$$t=T\bar{t},\qquad T:=\sqrt{\frac{(\rho+\rho')L}{(\rho-\rho')g}}=\sqrt{\frac{(1+R)L}{(1-R)g}},$$

where $R:=\rho'/\rho$ is the (dimensionless) density ratio $(0<R<1)$. The density-weighted potential difference is scaled as

$$\xi=aX\bar{\xi},\qquad X:=\sqrt{(\rho-\rho')(\rho+\rho')gL},$$

and we define the dimensionless steepness parameter

$$\alpha:=\frac{a}{L}.$$

Denoting the nonlinear terms on the right hand side of (2.15) by F and J, respectively, where

$$\begin{aligned}
F &:= G'(\eta)M(\eta)G(\eta)[\xi] - G_0'M_0G_0\xi,\\
J &:= \frac{1}{2(1+(\partial_x\eta)^2)}\Big\{ -\rho(\partial_x M(\eta)G'(\eta)[\xi])^2\\
&\quad +\rho(G(\eta)M(\eta)G'(\eta)[\xi])^2 + 2\rho(\partial_x\eta)(\partial_x M(\eta)G'(\eta)[\xi])(G(\eta)M(\eta)G'(\eta)[\xi])\\
&\quad +\rho'(\partial_x M(\eta)G(\eta)[\xi])^2 - \rho'(G'(\eta)M(\eta)G(\eta)[\xi])^2\\
&\quad -2\rho'(\partial_x\eta)(\partial_x M(\eta)G(\eta)[\xi])(G'(\eta)M(\eta)G(\eta)[\xi])\Big\},
\end{aligned}$$

we can expand

$$F(\eta,\xi) = F(a\bar\eta, aX\bar\xi) = \sum_{n=1}^{\infty} C_n^F F_n(\bar\eta,\bar\xi)\alpha^n, \quad J(\eta,\xi) = J(a\bar\eta, aX\bar\xi) = \sum_{n=1}^{\infty} C_n^J J_n(\bar\eta,\bar\xi)\alpha^n,$$

where C_n^F and C_n^J are constants. With the above scalings and notation, (2.15) becomes

$$\partial_{\bar t}\bar\eta = |\bar D|\bar\xi + \alpha F_1(\bar\eta,\bar\xi) + \mathcal{O}(\alpha^2), \qquad \partial_{\bar t}\bar\xi = -\bar\eta + \alpha J_1(\bar\eta,\bar\xi) + \mathcal{O}(\alpha^2),$$

where

$$\begin{aligned}
F_1 &= \Big(\frac{\rho-\rho'}{\rho+\rho'}\Big)\Big[\bar\eta|\bar D|^2\bar\xi - (\partial_{\bar x}\bar\eta)(\partial_{\bar x}\bar\xi) - |\bar D|[\bar\eta|\bar D|\bar\xi]\Big],\\
J_1 &= \Big(\frac{\rho-\rho'}{2(\rho+\rho')}\Big)\left[(|\bar D|\bar\xi)^2 - (\partial_{\bar x}\bar\xi)^2\right].
\end{aligned}$$

We complete the derivation of our model by assuming that $\alpha \ll 1$, dropping the "bar" notation and neglecting terms of order $\mathcal{O}(\alpha^2)$. Thus, we arrive at our nondimensional weakly nonlinear model:

$$\partial_t\eta = |D|\xi + \alpha\Big(\frac{\rho-\rho'}{\rho+\rho'}\Big)\Big[\eta|D|^2\xi - (\partial_x\eta)(\partial_x\xi) - |D|[\eta|D|\xi]\Big], \tag{2.16a}$$

$$\partial_t\xi = -\eta + \alpha\Big(\frac{\rho-\rho'}{2(\rho+\rho')}\Big)\left[(|D|\xi)^2 - (\partial_x\xi)^2\right]. \tag{2.16b}$$

3 Numerical method

3.1 Numerical approximations

For a numerical approximation of solutions to (2.16) it is natural, in light of the lateral ($\lambda = 2\pi$) periodicity of solutions, to utilize a Fourier collocation approach [12]. In brief, we denote the equally spaced collocation points by

$$x_j = j(\Delta x) = j\Big(\frac{2\pi}{N_x}\Big), \qquad j = 0,1,\cdots,N_x-1$$

and approximate the solution $(\eta(x,t),\xi(x,t))$ by a (truncated) Fourier series of complex exponentials:

$$\eta^{N_x}(x,t) := \sum_{p=-N_x/2}^{N_x/2-1} \hat{\eta}_p^{N_x}(t) e^{ipx}, \qquad \xi^{N_x}(x,t) := \sum_{p=-N_x/2}^{N_x/2-1} \hat{\xi}_p^{N_x}(t) e^{ipx}.$$

In requiring that the residual vanishes at the grid points, we enforce (2.16) at the collocation points, x_j, which results in a system of $(2N_x)$ ordinary differential equations for the $\eta^{N_x}(x_j,t)$ and $\xi^{N_x}(x_j,t)$. These we approximate with a fourth-order Runge-Kutta scheme [3] which delivers approximate solutions at the time levels

$$t_m = m(\Delta t) = m\Big(\frac{T}{N_t}\Big), \qquad m = 0,1,\cdots,N_t.$$

Derivatives and Fourier multipliers are applied in Fourier space, e.g.,

$$|D|\eta \approx |D|\eta^{N_x} = \sum_{p=-N_x/2}^{N_x/2-1} |p| \hat{\eta}_p^{N_x}(t) e^{ipx}.$$

Products are performed pointwise in physical space and the Discrete Fourier Transform (DFT), accelerated by the Fast Fourier Transform (FFT) algorithm, is used to transform between physical and Fourier space [12].

3.2 Exact solutions for convergence study

To test our algorithm we examine temporal and spatial convergence against exact solutions of the linearized equations ((2.16) with $\mathcal{O}(\alpha)$ terms eliminated) and an exact traveling wave solution of the full model equations (2.16). These exact solutions are derived in the following two sections and the convergence results are presented in Section 4.

3.2.1 Exact solutions for linear water waves

The linearization of (2.16) (where terms of order $\mathcal{O}(\alpha)$ are ignored) is easily seen to be

$$\partial_t \eta = |D|\xi, \tag{3.1a}$$

$$\partial_t \xi = -\eta, \tag{3.1b}$$

which we denote the "Linear Model". Using the Fourier series representations of η and ξ leads to

$$\partial_t \begin{pmatrix} \hat{\eta}_p \\ \hat{\xi}_p \end{pmatrix} = \begin{pmatrix} 0 & |p| \\ -1 & 0 \end{pmatrix} \begin{pmatrix} \hat{\eta}_p \\ \hat{\xi}_p \end{pmatrix},$$

where $\hat{\eta}_p$ and $\hat{\xi}_p$ are the p-th Fourier coefficients of η and ξ, respectively. Given initial conditions $(\eta_0(x),\xi_0(x))$, it is not difficult to show that the exact solution for wavenumbers $p>0$ is

$$\begin{pmatrix} \hat{\eta}_p(t) \\ \hat{\xi}_p(t) \end{pmatrix} = \begin{pmatrix} \hat{\eta}_p(0)\cos(\omega_p t) + \hat{\xi}_p(0)\omega_p \sin(\omega_p t) \\ \hat{\xi}_p(0)\cos(\omega_p t) - \hat{\eta}_p(0)\dfrac{1}{\omega_p}\sin(\omega_p t) \end{pmatrix}, \tag{3.2a}$$

where the dispersion relation is given by

$$\omega_p^2 := |p|.$$

At wavenumber $p=0$ we have the formulas

$$\begin{pmatrix} \hat{\eta}_0(t) \\ \hat{\xi}_0(t) \end{pmatrix} = \begin{pmatrix} \hat{\eta}_0(0) \\ \hat{\xi}_0(0) - \hat{\eta}_0(0)t \end{pmatrix}. \tag{3.2b}$$

3.2.2 Traveling wave solutions

To find a class of exact solutions to the *full* set of model equations, (2.16), we begin by changing to a reference frame moving uniformly with velocity $c \in \mathbf{R}$. Seeking steady solutions in this frame will yield traveling wave solutions which satisfy

$$c\partial_x \eta - |D|\xi = \alpha\left(\frac{\rho-\rho'}{\rho+\rho'}\right)\left[\eta|D|^2\xi - (\partial_x\eta)(\partial_x\xi) - |D|[\eta|D|\xi]\right], \tag{3.3a}$$

$$c\partial_x \xi + \eta = \alpha\left(\frac{\rho-\rho'}{2(\rho+\rho')}\right)\left[(|D|\xi)^2 - (\partial_x\xi)^2\right]. \tag{3.3b}$$

To find solutions to (3.3), we expand the solution (η,ξ,c) in Taylor series in the (small) parameter α:

$$\eta(x;\alpha) = \sum_{n=0}^{\infty} \eta_n(x)\alpha^n, \qquad \xi(x;\alpha) = \sum_{n=0}^{\infty} \xi_n(x)\alpha^n, \qquad c(\alpha) = \sum_{n=0}^{\infty} c_n\alpha^n. \tag{3.4}$$

Inserting these expansions (3.4), which can be shown to be strongly convergent, into (3.3) we equate at matching orders of α. At order $n=0$ we find

$$\begin{aligned} c_0\partial_x\eta_0 - |D|\xi_0 &= 0, \\ c_0\partial_x\xi_0 + \eta_0 &= 0, \end{aligned}$$

or, alternatively,

$$A_{c_0,p}\hat{u}_{0,p} = \begin{pmatrix} c_0(ip) & -|p| \\ 1 & c_0(ip) \end{pmatrix}\begin{pmatrix} \hat{\eta}_{0,p} \\ \hat{\xi}_{0,p} \end{pmatrix} = \begin{pmatrix} 0 \\ 0 \end{pmatrix}, \tag{3.5}$$

where

$$A_{c,p} := \begin{pmatrix} c(ip) & -|p| \\ 1 & c(ip) \end{pmatrix}, \qquad \hat{u}_{n,p} := \begin{pmatrix} \hat{\eta}_{n,p} \\ \hat{\xi}_{n,p} \end{pmatrix}.$$

To obtain a non-trivial solution, $A_{c_0,p}$ must be singular, that is, the determinant function

$$\Lambda_{c_0,p} := -(c_0 p)^2 + |p|$$

must vanish. To arrange this we select a non-zero wavenumber p_0 and then choose

$$c_0 = \frac{\sqrt{|p_0|}}{p_0}.$$

With the pair (c_0,p_0), we can solve (3.5) to find a non-trivial solution:

$$\hat{u}_{0,p_0}=\beta\begin{pmatrix}|p_0|\\ ic_0p_0\end{pmatrix},$$

for any $\beta\in\mathbf{C}$. As we wish to have real-valued solutions, at wavenumber $p=-p_0$ we select the complex conjugate:

$$\hat{u}_{0,-p_0}=\bar{\hat{u}}_{0,p_0}.$$

At wavenumber $p=0$, (3.5) reduces to

$$\begin{pmatrix}0&0\\1&0\end{pmatrix}\begin{pmatrix}\hat{\eta}_{0,0}\\ \hat{\xi}_{0,0}\end{pmatrix}=\begin{pmatrix}0\\0\end{pmatrix}.$$

For consistency, we enforce

$$\hat{\eta}_{0,0}=0,$$

which simply sets the mean water level. There are no restrictions on $\hat{\xi}_{0,0}$ so, for convenience, we choose

$$\hat{\xi}_{0,0}=0.$$

We note that this is no great restriction as it is the *gradient* of the potential which is important in the evolution equations so any constant term is effectively meaningless. When $p\neq 0,\pm p_0$, $A_{c_0,p}$ is non-singular and the unique solution is trivial:

$$\hat{u}_{0,p}=0.$$

At order $n>0$, (3.3) implies

$$\begin{aligned}c_0\partial_x\eta_n-|D|\xi_n=&\left(\frac{\rho-\rho'}{\rho+\rho'}\right)\Big[\sum_{l=0}^{n-1}\eta_{n-1-l}|D|^2\xi_l-\sum_{l=0}^{n-1}(\partial_x\eta_{n-1-l})(\partial_x\xi_l)\\&-\sum_{l=0}^{n-1}|D|\left[\eta_{n-1-l}|D|\xi_l\right]\Big]-c_n\partial_x\eta_0-\sum_{l=1}^{n-1}c_{n-l}\partial_x\eta_l,\\ c_0\partial_x\xi_n+\eta_n=&\left(\frac{\rho-\rho'}{2(\rho+\rho')}\right)\Big[\sum_{l=0}^{n-1}(|D|\xi_{n-1-l})(|D|\xi_l)-\sum_{l=0}^{n-1}(\partial_x\xi_{n-1-l})(\partial_x\xi_l)\Big]\\&-c_n\partial_x\xi_0-\sum_{l=1}^{n-1}c_{n-l}\partial_x\xi_l.\end{aligned}$$

Appealing to the Fourier series for (η_n,ξ_n) we can express this as

$$A_{c_0,p}\hat{u}_{n,p}=\hat{R}_{n,p}-c_n(ip)\hat{u}_{0,p}, \tag{3.6}$$

where

$$\hat{R}^{\eta}_{n,p} := \left(\frac{\rho-\rho'}{\rho+\rho'}\right)\Big[\sum_{l=0}^{n-1}\eta_{n-1-l}|D|^2\xi_l - \sum_{l=0}^{n-1}(\partial_x\eta_{n-1-l})(\partial_x\xi_l) - \sum_{l=0}^{n-1}|D|[\eta_{n-1-l}|D|\xi_l]\Big] - \sum_{l=1}^{n-1}c_{n-l}\partial_x\eta_l,$$

$$\hat{R}^{\xi}_{n,p} := \left(\frac{\rho-\rho'}{2(\rho+\rho')}\right)\Big[\sum_{l=0}^{n-1}(|D|\xi_{n-1-l})(|D|\xi_l) - \sum_{l=0}^{n-1}(\partial_x\xi_{n-1-l})(\partial_x\xi_l)\Big] - \sum_{l=1}^{n-1}c_{n-l}\partial_x\xi_l.$$

Given our choice of c_0, the matrix $A_{c_0,p}$ is, of course, singular at wavenumbers $p=\pm p_0$. Additionally, $A_{c_0,0}$ is also singular, so in order to solve (3.6) we consider three cases: $p=\pm p_0$, $p=0$ and $p\neq 0,\pm p_0$. In more detail:

1. **[Case 1:** $p=\pm p_0$**]** As we have mentioned, A_{c_0,p_0} is singular, however, the undetermined parameter c_n can be used to find a solution. To ensure consistency of the system we pick:
$$c_n = \frac{\hat{R}^{\eta}_{n,p_0} - ic_0p_0\hat{R}^{\xi}_{n,p_0}}{ip_0\hat{\eta}_{0,p_0} + c_0p_0^2\hat{\xi}_{0,p_0}}.$$
For uniqueness, we implement Stokes' strategy (see [28,29]) by requiring that $\hat{\eta}_n$ be L^2-orthogonal to $\hat{\eta}_0$. Since $\hat{\eta}_{0,p}=0$ for all $p\neq\pm p_0$ this condition amounts to
$$\hat{\eta}_{n,p_0} = \hat{\eta}_{n,-p_0} = 0.$$
With these choices
$$\hat{\xi}_{n,p_0} = \frac{\hat{R}^{\xi}_{n,p_0} - c_n(ip_0)\hat{\xi}_{0,p_0}}{ic_0p_0}$$
and $\hat{\xi}_{n,-p_0} = \bar{\hat{\xi}}_{n,p_0}$.
2. **[Case 2:** $p=0$**]** At order $n=0$ we set $\hat{u}_{0,p}=0$, therefore, (3.6) reduces to
$$A_{c_0,0}\hat{u}_{n,0} = \hat{R}_{n,0},$$
or,
$$\begin{pmatrix}0 & 0\\ 1 & 0\end{pmatrix}\begin{pmatrix}\hat{\eta}_{n,0}\\ \hat{\xi}_{n,0}\end{pmatrix} = \begin{pmatrix}\hat{R}^{\eta}_{n,0}\\ \hat{R}^{\xi}_{n,0}\end{pmatrix}.$$
It can be shown that $\hat{R}^{\eta}_{n,0}=0$ [17] so our system is consistent. The second equation reduces to
$$\hat{\eta}_{n,0} = \hat{R}^{\xi}_{n,0}$$
and to specify a unique solution we follow the strategy of the $n=0$ case and choose
$$\hat{\xi}_{n,0} = 0.$$

3. **[Case 3:** $p\neq 0,\pm p_0$**]** In this case (3.6) reduces to

$$A_{c_0,p}\hat{u}_{n,p}=\hat{R}_{n,p}$$

and, as $A_{c_0,p}$ is non-singular, this can be solved uniquely:

$$\hat{u}_{n,p}=\frac{1}{\Lambda_{c_0,p}}\begin{pmatrix} ic_0p\hat{R}^{\eta}_{n,p}+|p|\hat{R}^{\xi}_{n,p} \\ -\hat{R}^{\eta}_{n,p}+ic_0p\hat{R}^{\xi}_{n,p}\end{pmatrix}.$$

To give a feel for what one of these traveling wave solutions looks like, we plot, in Fig. 2, the shape, η, of such a wave versus x. Here we chose $N_x=64$, $N=20$ and $\alpha=1/100$.

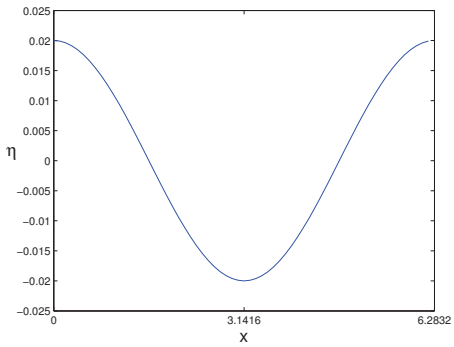

Figure 2: Plot of a traveling wave versus x at $\alpha=1/100$ with $N_x=64$ and $N=20$.

4 Numerical results

To begin we validate our code by studying convergence of our numerical solutions to the exact solutions we derived in the previous section, (3.2) or (3.4). Denoting either of these two families of exact solutions by $\{\eta_{\text{exact}},\xi_{\text{exact}}\}$. We measure the errors

$$\eta_{\text{error}}:=\left|\eta_{\text{exact}}(x,T)-\eta^{N_x}(x,T)\right|_{L^\infty_x}, \tag{4.1a}$$

$$\xi_{\text{error}}:=\left|\xi_{\text{exact}}(x,T)-\xi^{N_x}(x,T)\right|_{L^\infty_x}, \tag{4.1b}$$

where $T=N_t(\Delta t)$ is the final time of our simulation. For all simulations we choose the values $T=10$, $\lambda=2\pi$, while the initial conditions for the Linear Model (3.1) are

$$\eta_0(x)=e^{\cos(x)},\qquad \xi_0(x)=e^{\sin(x)},$$

and the traveling wave found in Section 3.2.2 serves as the initial condition for the weakly nonlinear model (2.16). The traveling wave solution is approximated by

$$\eta^N(x;\alpha):=\sum_{n=0}^{N}\eta_n(x)\alpha^n,\qquad \xi^N(x;\alpha):=\sum_{n=0}^{N}\xi_n(x)\alpha^n,\qquad c^N(\alpha):=\sum_{n=0}^{N}c_n\alpha^n,$$

for which we set $N=20$ and $\alpha=0.01$.

4.1 Temporal convergence

To examine temporal convergence we determine the errors for a fixed, highly resolved, spatial discretization $N_x=64$ ($\Delta x\approx 0.09817$), as Δt is refined. For physical parameters we choose

$$\lambda=2\pi,\quad T=10,\quad \rho'=1,\quad \rho=2,\quad p_0=1,\quad \alpha=0.01,$$

and use $N=20$ for the traveling wave solutions. The Runge-Kutta time-stepping algorithm has a global error of $\mathcal{O}((\Delta t)^4)$ [3], therefore we should observe a slope of four on a log-log plot of error versus Δt. Using a least squares algorithm to fit our "experimental" data we find values that are almost exactly four. Figs. 3 and 4 further demonstrate that the desired slope was achieved for the Linear Model and traveling waves, respectively. In Tables 1 and 2 we present the raw data of these experiments. In the right two columns of Table 2 we supplement this, in the case of the traveling waves, with data from a more "realistic" simulation with densities $\rho'=1.0079$, $\rho=1.0201$ [24].

Table 1: Error results for the Linear Model: Temporal convergence analysis.

Δt	η_{error}	ξ_{error}
0.08	1.0218×10^{-5}	9.8617×10^{-6}
0.04	6.3132×10^{-7}	6.3697×10^{-7}
0.02	3.9311×10^{-8}	4.0419×10^{-8}
0.01	2.4518×10^{-9}	2.5447×10^{-9}
0.005	1.5307×10^{-10}	1.5970×10^{-10}
0.0025	9.5579×10^{-12}	1.0088×10^{-11}

Table 2: Error results for traveling waves: Temporal convergence analysis.

	$\rho'=1,\rho=2$		$\rho'=1.0079,\rho=1.0201$	
Δt	η_{error}	ξ_{error}	η_{error}	ξ_{error}
0.08	6.8371×10^{-8}	6.8566×10^{-8}	6.8253×10^{-8}	6.8256×10^{-8}
0.04	4.2720×10^{-9}	4.2818×10^{-9}	4.2620×10^{-9}	4.2622×10^{-9}
0.02	2.6717×10^{-10}	2.6779×10^{-10}	2.6655×10^{-10}	2.6656×10^{-10}
0.01	1.6702×10^{-11}	1.6741×10^{-11}	1.6663×10^{-11}	1.6664×10^{-11}
0.005	1.0440×10^{-12}	1.0465×10^{-12}	1.0415×10^{-12}	1.0415×10^{-12}
0.0025	6.5201×10^{-14}	6.5474×10^{-14}	6.5200×10^{-14}	6.5040×10^{-14}

4.2 Spatial convergence

For our investigation of spatial convergence we fix the temporal discretization to the highly resolved value $N_t=4000$ ($\Delta t=0.0025$) and simulate solutions for $N_x=2^j$, $j=2,\cdots,6$. Once again we select

$$\lambda=2\pi,\quad T=10,\quad \rho'=1,\quad \rho=2,\quad p_0=1,\quad \alpha=0.01,$$

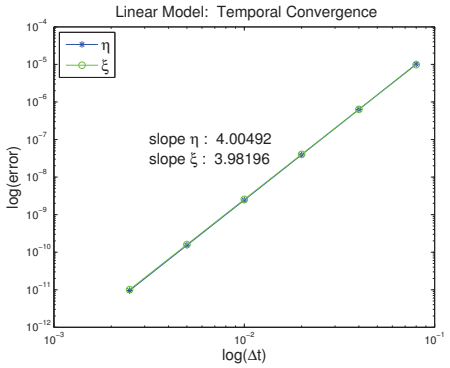

Figure 3: Temporal convergence for the Linear Model.

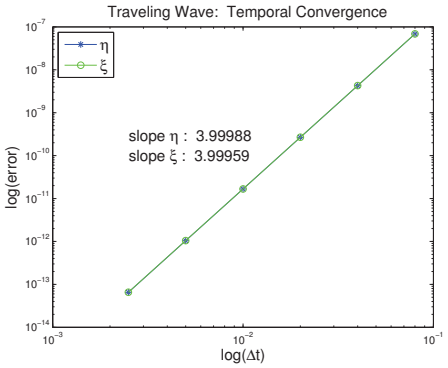

Figure 4: Temporal convergence for traveling waves.

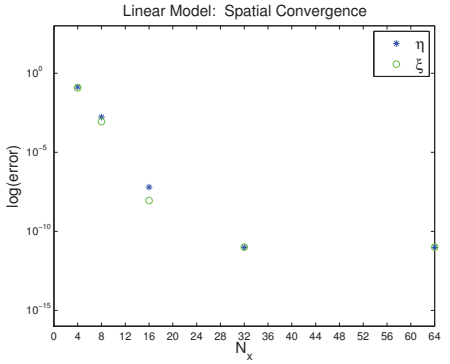

Figure 5: Spatial convergence for the Linear Model.

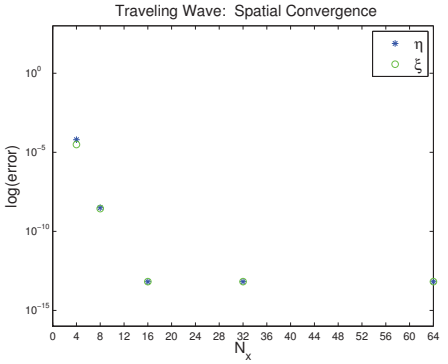

Figure 6: Spatial convergence for the traveling waves.

and $N=20$ for the traveling waves. In our simulations we find the spectral convergence results that such methods generate for smooth solutions [12]. The error results are presented graphically in Figs. 5 and 6 and as raw data in Tables 3 and 4. Again, in the right two columns of Table 4 we supplement this, in the case of the traveling waves, with data from a more "realistic" simulation with densities $\rho'=1.0079$, $\rho=1.0201$ [24].

Table 3: Error results for the Linear Model: Spatial convergence analysis.

N_x	η_{error}	ξ_{error}
4	1.3438×10^{-1}	1.2002×10^{-1}
8	1.6651×10^{-3}	8.5868×10^{-4}
16	6.2002×10^{-8}	8.8060×10^{-9}
32	9.5586×10^{-12}	1.0088×10^{-11}
64	9.5584×10^{-12}	1.0090×10^{-11}

Table 4: Error results for traveling waves: Spatial convergence analysis.

	$\rho'=1, \rho=2$		$\rho'=1.0079, \rho=1.0201$	
N_x	η_{error}	ξ_{error}	η_{error}	ξ_{error}
4	6.2182×10^{-5}	3.0626×10^{-5}	1.0989×10^{-6}	4.9214×10^{-6}
8	3.1234×10^{-9}	2.7171×10^{-9}	8.1384×10^{-14}	7.9574×10^{-14}
16	6.5207×10^{-14}	6.5406×10^{-14}	6.5189×10^{-14}	6.5116×10^{-14}
32	6.5328×10^{-14}	6.5557×10^{-14}	6.5070×10^{-14}	6.5070×10^{-14}
64	6.5200×10^{-14}	6.5472×10^{-14}	6.5196×10^{-14}	6.5035×10^{-14}

4.3 Weakly nonlinear model

To conclude our numerical experiments we examine the wave-packet profiles considered by Craig & Sulem [10] in their seminal work on OE methods for the classical single-fluid water-wave problem. For this we specify the nondimensional initial data

$$\eta_0(x)=e^{-(4/3)(x-\pi)^2}\cos(10x), \qquad \xi_0(x)=0, \tag{4.2}$$

with $\alpha=0.01$. In these simulations we select a final time of $T=10$ and numerical parameters N_t=4000 and N_x=128 (Δt=0.0025 and $\Delta x\approx$0.04909) which deliver excellent accuracy and stability. To validate these computations we compute the total energy (Hamiltonian) of our model system. To obtain this we recall [6,8] that the Hamiltonian of the *full* set of evolution equations (2.15) is

$$H_{\text{full}}(\eta,\xi)=\frac{1}{2}\int_0^\lambda \xi\big(G(\eta)M(\eta)G'(\eta)\xi\big)+g(\rho-\rho')\eta^2 dx,$$

where the first term is the kinetic energy of the system and the second gives the potential energy. The total energy for solutions of our model system (2.16) can be recovered by nondimensionalization and retaining only terms in the expansion of the operators to order one, resulting in

$$H(\eta,\xi)=\frac{1}{2}\int_0^{2\pi}\xi\Big(|D|\xi+\alpha\Big(\frac{\rho-\rho'}{\rho+\rho'}\Big)\Big[\eta|D|^2\xi-(\partial_x\eta)(\partial_x\xi)-|D|[\eta|D|\xi]\Big]\Big)+\eta^2 dx.$$

We define the relative energy defect by

$$E_{\text{error}}:=\frac{|H(\eta_0(x),\xi_0(x))-H(\eta(x,T),\xi(x,T))|}{H(\eta_0(x),\xi_0(x))},$$

and display in Table 5 values of this error measure after $T=10$ units of time.

We notice that as the nonlinear parameter α is increased to 0.1 our code becomes somewhat unreliable and some type of filtering mechanism is required (as it was in the work of Craig & Sulem [10]).

Table 5: Energy defect versus nonlinearity parameter α.

α	E_{error}
0.001	1.4108×10^{-11}
0.01	1.4201×10^{-11}
0.1	1.3550×10^{-1}

We conclude by choosing values of the density parameters suggested by the literature (see Mercier, Vasseur and Dauxios [24]). For this we select

$$\lambda=2\pi,\quad T=10,\quad \rho'=1.0079,\quad \rho=1.0201,\quad p_0=1,\quad \alpha=0.01,$$

and set $N_x=128$ and $N_t=4000$. In Figs. 7 and 8 we depict the evolution of η and ξ, respectively, as t increases from $t_0=0$ to $T=10$ which qualitatively shows the same behavior observed by Craig & Sulem [10] for the classical water-wave problem.

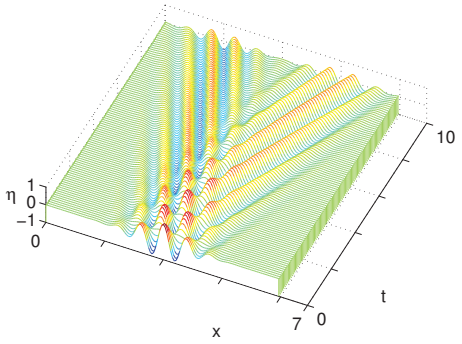

Figure 7: Evolution of the interface quantity η for the weakly nonlinear model for the wave packet (4.2).

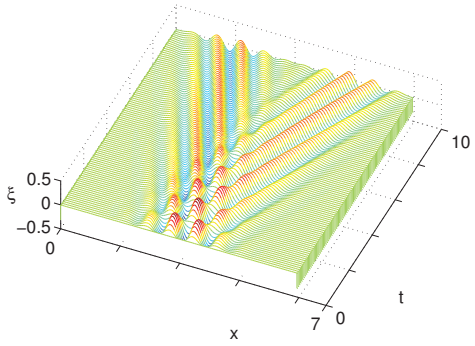

Figure 8: Evolution of the interface quantity ξ for the weakly nonlinear model for the wave packet (4.2).

Acknowledgments

DPN gratefully acknowledges support from the National Science Foundation through grant No. DMS-0810958 and the Department of Energy under Award No. DE-SC0001549.

Disclaimer: This report was prepared as an account of work sponsored by an agency of the United States Government. Neither the United States Government nor any agency thereof, nor any of their employees, make any warranty, express or implied, or assumes any legal liability or responsibility for the accuracy, completeness, or usefulness of any information, apparatus, product, or process disclosed, or represents that its use would not infringe privately owned rights. Reference herein to any specific commercial product, process, or service by trade name, trademark, manufacturer, or otherwise does not necessarily constitute or imply its endorsement, recommendation, or favoring by the United

States Government or any agency thereof. The views and opinions of authors expressed herein do not necessarily state or reflect those of the United States Government or any agency thereof.

References

[1] T. B. Benjamin and T. J. Bridges, Reappraisal of the Kelvin-Helmholtz problem I-Hamiltonian structure, J. Fluid Mech., 333 (1997), 301–325.
[2] T. B. Benjamin and T. J. Bridges, Reappraisal of the Kelvin-Helmholtz problem II-interaction of the Kelvin-Helmholtz, superharmonic and Benjamin-Feir instabilities, J. Fluid Mech., 333 (1997), 327–373.
[3] R. Burden and J. D. Faires, Numerical Analysis, Brooks/Cole Publishing Co., Pacific Grove, CA, sixth edition, 1997.
[4] J. L. Bona, D. Lannes and J.-C. Saut, Asymptotic models for internal waves, J. Math. Pures Appl., 89(6) (2008), 538–566.
[5] W. Choi and R. Camassa, Weakly nonlinear internal waves in a two-fluid system, J. Fluid Mech., 313 (1996), 83–103.
[6] W. Craig and M. D. Groves, Normal forms for wave motion in fluid interfaces, Wave Motion, 31(1) (2000), 21–41.
[7] W. Craig, P. Guyenne and H. Kalisch, A new model for large amplitude long internal waves, Comptes Rendus Mechanique, 332(7) (2004), 525–530.
[8] W. Craig, P. Guyenne and H. Kalisch, Hamiltonian long-wave expansions for free surfaces and interfaces, Commun. Pure Appl. Math., 58(12) (2005), 1587–1641.
[9] R. Coifman and Y. Meyer, Nonlinear harmonic analysis and analytic dependence, in Pseudodifferential Operators and Applications (Notre Dame, Ind., 1984), pages 71–78, Amer. Math. Soc., 1985.
[10] W. Craig and C. Sulem, Numerical simulation of gravity waves, J. Comput. Phys., 108 (1993), 73–83.
[11] P. Guyenne, D. Lannes and J.-C. Saut, Well-posedness of the Cauchy problem for models of large amplitude internal waves, Nonlinearity, 23(2) (2010), 237–275.
[12] D. Gottlieb and S. A. Orszag, Numerical analysis of spectral methods: theory and applications, Society for Industrial and Applied Mathematics, Philadelphia, Pa., 1977, CBMS-NSF Regional Conference Series in Applied Mathematics, No. 26.
[13] T. S. Haut and M. J. Ablowitz, A reformulation and applications of interfacial fluids with a free surface, J. Fluid Mech., 631 (2009), 375–396.
[14] K. Helfrich and W. Melville, Long nonlinear internal waves, Ann. Rev. Fluid Mech., 38 (2006), 395–425.
[15] C. R. Jackson, The internal wave altas, `http://internalwavealtas.com`.
[16] C. G. Koop and G. Butler, An investigation of internal solitary waves in a two-fluid system, J. Fluid Mech., 112 (1981), 225–251.
[17] M. Kakleas and D. P. Nicholls, Numerical simulation of a weakly nonlinear model for water waves with viscosity, J. Sci. Comput., 42(2) (2010), 274–290.
[18] H. Lamb, Hydrodynamics, Cambridge University Press, Cambridge, sixth edition, 1993.
[19] C. C. Mei, Numerical methods in water-wave diffraction and radiation, Ann. Rev. Fluid Mech., 10 (1978), 393–416.
[20] D. M. Milder, An improved formalism for rough-surface scattering of acoustic and electromagnetic waves, in Proceedings of SPIE-The International Society for Optical Engineering

(San Diego, 1991), volume 1558, pages 213–221, Int. Soc. for Optical Engineering, Bellingham, WA, 1991.
[21] D. M. Milder, An improved formalism for wave scattering from rough surfaces, J. Acoust. Soc. Am., 89(2) (1991), 529–541.
[22] D. M. Milder and H. T. Sharp, Efficient computation of rough surface scattering, in Mathematical and Numerical Aspects of Wave Propagation Phenomena (Strasbourg, 1991), pages 314–322, SIAM, Philadelphia, PA, 1991.
[23] D. M. Milder and H. T. Sharp, An improved formalism for rough surface scattering II: numerical trials in three dimensions, J. Acoust. Soc. Am., 91(5) (1992), 2620–2626.
[24] M. J. Mercier, R. Vasseur and T. Dauxois, Resurrecting dead-water phenomenon, Nonlinear Pro. Geophys., 18 (2011), 193–208.
[25] H. Y. Nguyen and F. Dias, A Boussinesq system for two-way propagation of interfacial waves, Phys. D, 237(18) (2008), 2365–2389.
[26] D. P. Nicholls, Boundary perturbation methods for water waves, GAMM-Mitteilungen, 30(1) (2007), 44–74.
[27] D. P. Nicholls and F. Reitich, A new approach to analyticity of Dirichlet-Neumann operators, Proc. Roy. Soc. Edinburgh Sec. A, 131(6) (2001), 1411–1433.
[28] D. P. Nicholls and F. Reitich, On analyticity of traveling water waves, Proc. Roy. Soc. Lond. A, 461(2057) (2005), 1283–1309.
[29] D. P. Nicholls and F. Reitich, Rapid, stable, high-order computation of traveling water waves in three dimensions, Euro. J. Mech. B Fluids, 25(4) (2006), 406–424.
[30] R. Scardovelli and S. Zaleski, Direct numerical simulation of free-surface and interfacial flow, Ann. Rev. Fluid Mech., 31 (1999), 567–603.
[31] W.-T. Tsai and D. K. P. Yue, Computation of nonlinear free-surface flows, in Ann. Rev. Fluid Mech., 28, 249–278, Annual Reviews, Palo Alto, CA, 1996.
[32] R. W. Yeung, Numerical methods in free-surface flows, Ann. Rev. Fluid Mech., 14 (1982), 395–442.
[33] V. Zakharov, Stability of periodic waves of finite amplitude on the surface of a deep fluid, J. Appl. Mech. Tech. Phys., 9 (1968), 190–194.